

# EVALUATION OF ISOLATED FUSELAGE AND ROTOR-FUSELAGE INTERACTION USING CFD

**Thomas RENAUD**

[thomas.renaud@onera.fr](mailto:thomas.renaud@onera.fr)

Research Engineer

Office National d'Etudes et Recherches Aérospatiales, Châtillon, France

**David O'BRIEN**

Graduate Research Assistant

[gtg770d@prism.gatech.edu](mailto:gtg770d@prism.gatech.edu)

Georgia Institute of Technology, Atlanta, GA, USA

**Marilyn SMITH**

Associate Professor

[marilyn.smith@ae.gatech.edu](mailto:marilyn.smith@ae.gatech.edu)

**Mark POTSDAM**

[mpotsdam@mail.arc.nasa.gov](mailto:mpotsdam@mail.arc.nasa.gov)

Aerospace Engineer

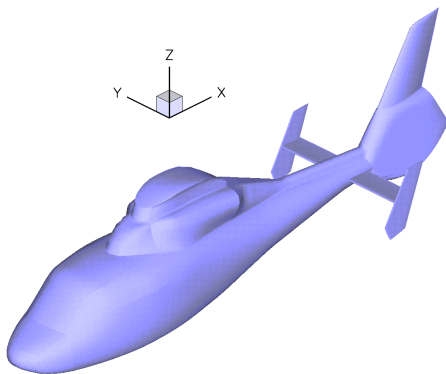
US Army Aeroflightdynamics Directorate (AMRDEC), Moffett Field, CA, USA

## ABSTRACT

The US Army Aeroflightdynamics Directorate (AFDD), the French Office National d'Etudes et de Recherches Aérospatiales (ONERA) and the Georgia Institute of Technology (GIT) are working under the United States/France Memorandum of Agreement on Helicopter Aeromechanics to study rotorcraft aeromechanics issues of interest to both nations. As a task under this agreement, a comparative study of the Dauphin 365N helicopter has been undertaken to analyze the capabilities and weaknesses of state-of-the-art computational fluid dynamics (CFD) codes, with the aim of fuselage performance prediction and investigation of rotor-fuselage interaction. Three CFD flow solvers applied on three meshes provide similar results in terms of pressure coefficient. Force predictions vary somewhat. This paper presents details on the grid sensitivity and the low Mach number preconditioning influence. The importance of taking into account the wind tunnel strut and the rotor hub is shown. The pressure coefficients along top and bottom centerlines of the fuselage are in good agreement with the experiment except in the area aft of the hub. There remains a discrepancy between the computed forces and the experimental data due in part to modelling inaccuracies. Rotor-fuselage interactions are performed using uniform and non-uniform actuator disk models in order to simulate the rotor downwash.

## NOTATIONS

Reference frame:



$$C_D S = \frac{\text{Drag}}{0.5 \rho_\infty V_\infty^2} : \text{drag force coefficient, m}^2$$

$$C_S S = \frac{\text{Side}}{0.5 \rho_\infty V_\infty^2} : \text{side force coefficient, m}^2$$

$$C_L S = \frac{\text{Lift}}{0.5 \rho_\infty V_\infty^2} : \text{lift force coefficient, m}^2$$

$$C_P = \frac{p - p_\infty}{0.5 \rho_\infty V_\infty^2} : \text{pressure coefficient}$$

$200C_T/\sigma$  : rotor thrust

Re : Reynolds number

S : rotor disk area, m<sup>2</sup>

$V_\infty$  : freestream velocity, m/s

$\alpha$  : pitch angle, degrees

$\beta$  : sideslip angle, degrees

$\beta$  : Low Mach number preconditioning parameter

$\rho_\infty$  : freestream fluid density

Presented at the American Helicopter Society 60<sup>th</sup> Annual Forum, Baltimore, MD, June 7-10, 2004.

Copyright © 2004 by the American Helicopter Society International, Inc. All rights reserved.

## INTRODUCTION

The application of Computational Fluid Dynamics (CFD) for rotorcraft analysis and design has been subject to questions concerning the efficiency and accuracy of methodologies to capture complex flow physics about realistic fuselage configurations. However, this is an important research topic since fuselage drag has been shown to account for up to one-third of total helicopter drag. In addition, the rotor should be included in any numerical simulations since rotor-fuselage interactions are complex and may have a major influence on the helicopter flow field physics.

Under the United States/France Memorandum of Agreement on Helicopter Aeromechanics, the US Army Aeroflightdynamics Directorate (AFDD), the French Office National d'Etudes et de Recherches Aérospatiales (ONERA) and the Georgia Institute of Technology (GIT) are performing cooperative research to study rotorcraft aeromechanics of interest to both nations. As part of this agreement, a comparative study of the Dauphin 365N helicopter has been undertaken to analyze the capabilities and the weaknesses of state-of-the-art CFD codes. Since 1992, ONERA has used a model of the Dauphin helicopter equipped with a powered main rotor in the S2Ch and more recently in the F1 wind tunnels. ONERA has made available the experimental results that include balance forces and moments data, fuselage pressure coefficients, and Laser Doppler Velocimetry (LDV) measurements of the wake. The three partners have run their own CFD codes on their own grids for several different configurations.

## NUMERICAL METHODS

### OVERFLOW 2.0

AFDD calculations use the Reynolds-averaged Navier-Stokes (RANS) computational fluid dynamics code OVERFLOW 2.0 [1, 2, 3]. It offers numerous spatial and temporal algorithmic options, turbulence models, and boundary conditions. Low Mach number preconditioning (LMP) is available [4] employing the formulation of Merkle and Choi [5]. In the Chimera domain decomposition methodology, geometrically complex configurations are reduced to a set of relatively simple overlapping grids. Solutions are computed on node-centred, structured, overset grids made up of body-conforming "near-body" grids and automatically generated Cartesian "off-body" grids. For the calculations on the Dauphin, OVERFLOW 2.0 runs use 2<sup>nd</sup>-order spatial central differencing with 4<sup>th</sup>-order matrix artificial dissipation and an implicit 1<sup>st</sup>-order temporal scheme. Runs are made with a constant CFL number, typically 3 to 6. Low Mach number preconditioned calculations use the standard LMP parameter  $\beta M_\infty^2$  with  $\beta=3$ . The Spalart-Allmaras,  $k-\omega$ , and Menter SST turbulence models are

used in the near-body grids, which are assumed fully turbulent. A thin layer approximation is used, and viscous terms are activated only in the wall normal direction. Off-body grids are modelled as inviscid in order to reduce the numerical dissipation in the wake. Both the domain connectivity and flow solver modules have been parallelized for efficient, scalable computations on large parallel computers or a network of PCs/workstations using the MPI protocol. Solutions were computed on 16 processors of an IBM Power4. The equivalent processing rate on one processor is 12.4  $\mu\text{sec}/\text{node}/\text{iteration}$ . Runs typically require 2500 iterations for force and moment convergence.

### elsA

ONERA has utilized for this effort the object-oriented code, *elsA* [6] (Ensemble Logiciel de Simulation en Aérodynamique). The Reynolds-averaged Navier-Stokes equations are solved via a finite volume formulation. Multiblock structured meshes permit the efficient modelling of a wide variety of complex configurations (aircraft, turbomachinery, helicopter...). *elsA* uses a 2<sup>nd</sup> order discretization in space based on Jameson's scalar artificial viscosity with Martinelli's correction. Time integration is achieved by implicit LU scalar relaxation with a backward Euler scheme. As *elsA* solves the compressible Navier-Stokes equations, local preconditioning based on the Merkle and Choi formulation [5] is employed to avoid poor convergence rate and solution accuracy in the incompressible Mach number regime. A LMP parameter  $\beta=2$  has been used for the present computations. The *elsA* solver includes numerous turbulence models (Spalart-Allmaras, Smith  $k-l$ ,  $k-\omega$ ...) for applications with differing physics. A Chimera method [7] simplifies the process of mesh generation by using overlapping grids. Solutions were computed on one processor of a NEC SX-6. The mean required CPU time is about 6  $\mu\text{sec}/\text{node}/\text{iteration}$ . Runs typically require 2500 iterations for force and moment convergence.

### FUN3D

FUN3D solves the RANS equations using an implicit solver on unstructured tetrahedral meshes [11, 12, 13]. FUN3D is capable of computing solutions for both compressible and incompressible Mach regimes using a backward Euler time discretization. The resulting linear system of equations is solved using a point-implicit relaxation scheme. Incompressible flows are solved using the Chorin [14] artificial compressibility method. The turbulence is modelled by the Spalart-Allmaras model. FUN3D uses a node-based algorithm where flow variables are stored at the vertices of the cells. The RANS equations are solved on the non-overlapping control volumes that surround each node. Roe's flux difference splitting technique [15] is utilized to calculate the inviscid fluxes on the control volume faces, while viscous fluxes

are computed using a finite volume formulation that results in an equivalent central difference approximation. Solutions were computed on 16 375MHz processors of an IBM SP3. The mean required CPU time is 567  $\mu\text{sec}/\text{node}/\text{iteration}$  for the incompressible grids and 994  $\mu\text{sec}/\text{node}/\text{iteration}$  for the compressible actuator disk computations. Runs typically require 600 iterations for force and moment convergence.

### Actuator Disk Model

A rotating component such as a rotor, ducted fan or propeller can be simplified by modelling the rotor as a lifting surface called an “actuator disk”. An actuator disk can be implemented with a variety of conditions from a steady, constant pressure change computed from momentum theory to varying time-dependent forces extracted from a simpler aerodynamic method such as a comprehensive code. The coupling can be open-loop with no feedback to the original theory generating the initial rotor condition, or it can provide feedback via either loose or tight coupling. With any implementation of the actuator disk, a large reduction in computational cost is achieved in comparison with an unsteady Navier-Stokes computation of the flow around the individual rotating blades. This boundary condition is modelled via the use of momentum and energy source terms [8, 9, 10] in *elsA* and *OVERFLOW* or a characteristic type approach, similar to the one used by Fejtek and Roberts [16], in *FUN3D*.

The discontinuities across the actuator disk are calculated for this research by uniform momentum equilibrium using the total rotor thrust (Figure 1) or by using a lifting line method to provide momentum variations in the radial and azimuthal directions on the disk (non-uniform actuator disk). In the present study for the non-uniform actuator disk, the aerodynamic loads on the rotor are computed with the lifting line-based code *HOST* [21] from Eurocopter.

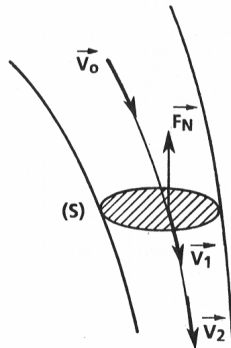


Figure 1. Representation of the flow downwash through an actuator disk with a global lift

### GRIDS

Due to the constraints of the individual numerical methods, the partners used their own grid around the

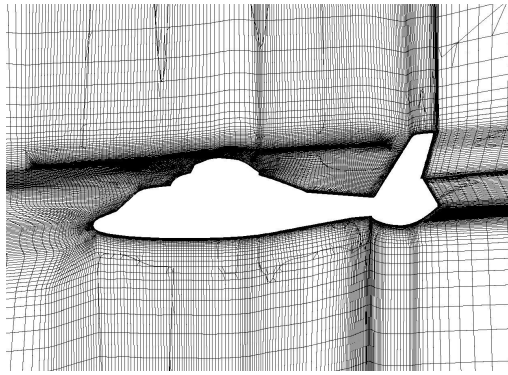
Dauphin 365N geometry. They tried to respect a minimal global number of 7 million points. The first grid point off the surface (.000011m) results in calculated  $y^+$  values typically less than 1. ONERA generated a multiblock grid with the *ICEM-CFD* software, where the actuator disk surface is directly meshed (Figure 2a). AFDD uses overset structured meshes, with near-body grids generated with the NASA-developed, overset grid generation software *OVERGRID* [2]. The viscous near-body grids extend out a distance of 10% of the fuselage length. Automatically generated Cartesian off-body grids extend to the farfield (Figure 2b). Finally, *VGrids* (v3.3) [17] and *Gridgen* (v15.0) [18] were used to generate tetrahedral grids needed for unstructured *FUN3D* computations. *GIT*'s strategy allows mesh refinement near the helicopter wall and in the actuator disk area (Figure 2c).

### MODEL AND EXPERIMENTS

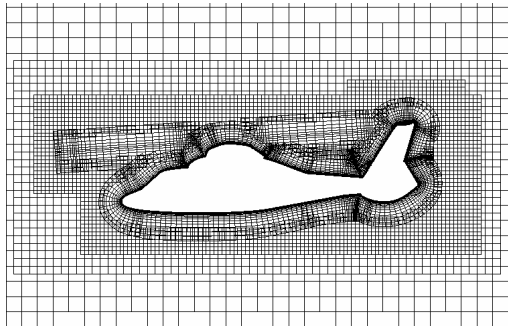
At ONERA, several wind tunnel tests on a Dauphin helicopter model equipped with a powered main rotor were performed in the 1990's in the S2Ch wind tunnel, which is now closed. Because of the rapidly improving numerical methods and computational power, further tests were warranted and have recently been carried out in the F1 subsonic wind tunnel [19].

The tested helicopter model is a 1/7.7 Dauphin model equipped with a powered main rotor of 1.5m diameter (Figure 3). The length of the fuselage is equal to 1.5m. Its rotor is articulated in pitch, flap and lead-lag motions. The rotor rotation is ensured by an electric engine which allows a blade tip speed of  $R\Omega=100\text{m/s}$ . A fuselage devoted to steady pressure measurements is equipped with 234 transducers. The fuselage model contains holes at the front and the rear parts of the engine fairing. In order to prevent binding of the balance, a small gap exists between the strut and the fuselage bottom surface. For pressure comparisons, these holes have been sealed so that the experimental geometry correlates more closely with the computational one, which does not model these gaps.

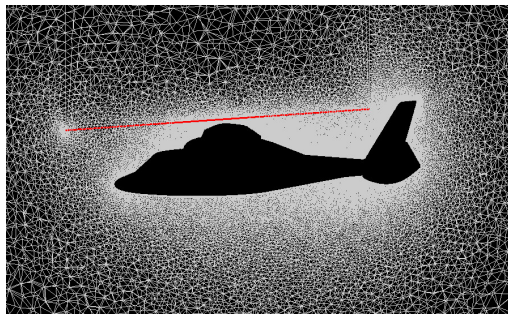
The S2Ch tests provide steady pressure measurements. Two balances measure the aerodynamic forces and moments for each part of the model: one balance measures the global forces on the fuselage and the rotor; the other one measures only the rotor. The subsequent and more detailed F1 tests provide more reliable pressure measurements for the test cases investigated in this paper, but only a single combined rotor and fuselage balance measurement.



a) ONERA



b) AFDD



c) GIT

Figure 2. Grids around fuselage and actuator disk



Figure 3. Dauphin helicopter model

## RESULTS

For this paper, two flight cases have been chosen in order to analyze the effect of numerical parameters, geometry and flow conditions. The first configuration has a freestream velocity of  $V_\infty=15$  m/s (0.044 Mach), a Reynolds number  $Re=1.07 \times 10^6$   $m^{-1}$ , an angle of incidence  $\alpha=-3^\circ$  and no sideslip. The second

configuration differs from the first one by an increase in the freestream velocity to  $V_\infty=30$  m/s and a sideslip angle  $\beta=-5^\circ$  (nose right). The test conditions for the fuselage with rotor correspond to the rotor thrust of  $200C_T/\sigma=14.5$ . The basic computed geometry does not take into account the rotor hub and the strut. Moreover, the engine fairing geometry has been simplified.

### Isolated Fuselage

#### Effect of Low Mach Number Preconditioning

The effect of low Mach number preconditioning for the Dauphin isolated fuselage test case without sideslip is initially studied. Both ONERA and AFDD solvers deal with compressible Navier-Stokes equations and use similar preconditioning methods. A comparison of the preconditioning influence – through the LMP (low Mach number preconditioning) parameter  $\beta$  – is presented in Figure 4. The goal is to provide as much preconditioning as possible to speed up the solution without compromising the accuracy of the solution. This is achieved by lowering the LMP parameter as much as possible. The drag, side and lift forces are plotted with respect to the preconditioning parameter. The ONERA and AFDD trends are in good agreement, in particular for drag and lift, for which asymptotic values are obtained. The importance and the necessity of using low speed preconditioning in such flow configurations is seen. The drag decreases by 200% and the lift increases by 83%. The GIT methodology is capable of solving either the incompressible or compressible Navier-Stokes equations and provides a consistent behaviour with respect to this analysis.

#### Grid Sensitivity

For the zero sideslip case, a grid sensitivity study was performed by AFDD and GIT. During this analysis, it was determined that the number of surface points plays a more important role than the global volume number of points when comparing solutions from disparate methods, such as those used here. Figure 5 shows the evolution of the drag, side and lift forces with respect to the number of surface points. Two ONERA runs – the fine baseline grid and a coarser grid (taking every other point) – are also plotted on the graphs. All three partners observe the same trends: when the mesh is refined, the drag force decreases whereas the side and lift forces increase. AFDD and GIT obtain similar grid convergence so that near-grid independence can be assumed.

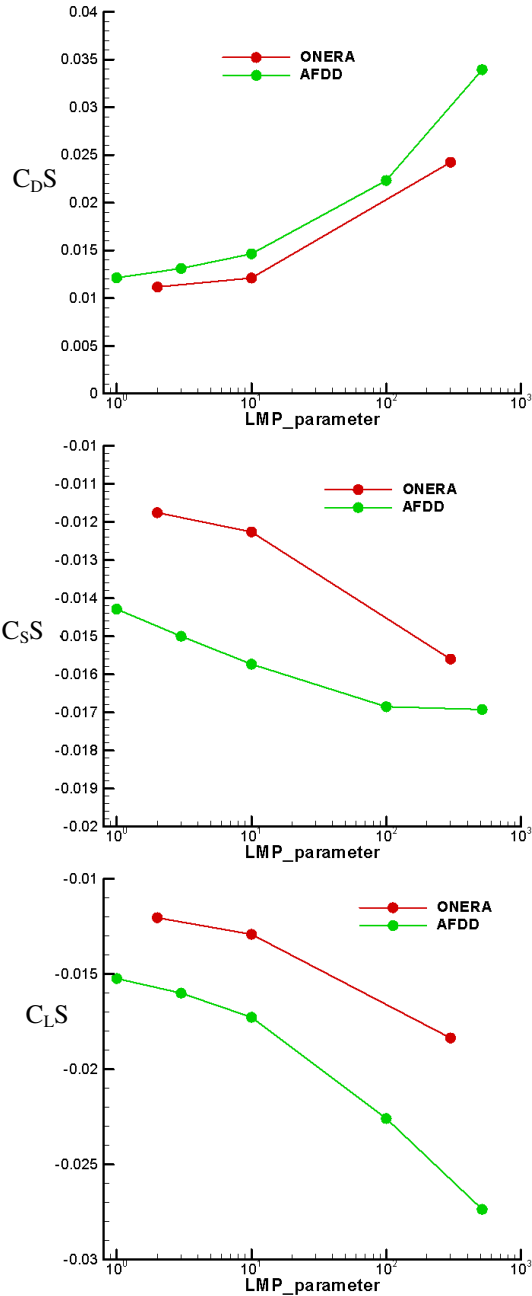


Figure 4. Influence of preconditioning on forces

Turbulence Model Effect

Figure 6 presents the ONERA comparison of three turbulence models (Spalart-Allmaras, k-l and k- $\omega$ ) on the pressure coefficient along the top centerline of the fuselage. The three numerical results are in very good agreement and compare well with the experiment on the upper centerline. S2Ch and F1 experimental data are plotted and show good agreement with each other. AFDD obtains similar results (not shown here) and no turbulence model is able to predict correctly the separation aft of the hub and engine fairing ( $X>0.7$ ).

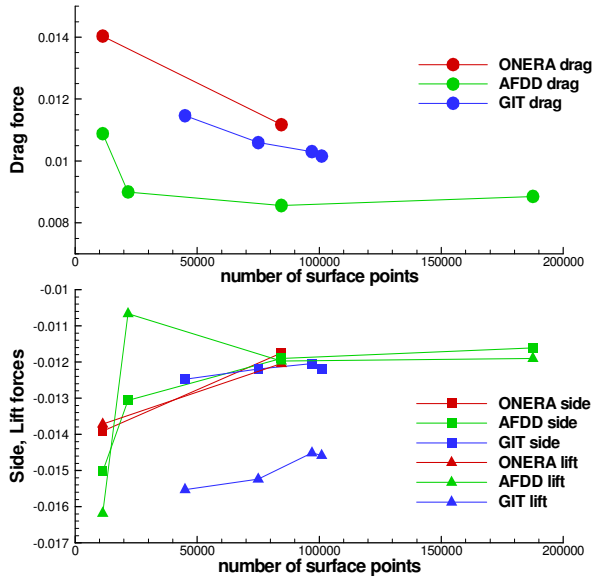


Figure 5. Grid sensitivity on forces

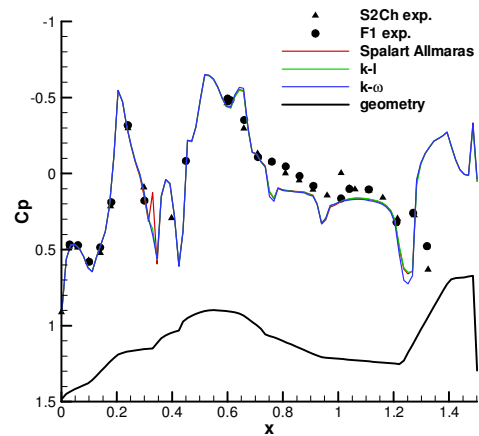


Figure 6. ONERA comparison of turbulence model effect on pressure coefficient along the top fuselage centerline

Pressure Coefficient Comparison

Figure 7 shows a comparison of pressure coefficients along the top and bottom centerlines for the three partners using the Spalart-Allmaras turbulence model. The numerical results are in good agreement with each other and with the experiments. On the upper centerline, there is a small discrepancy on the tail boom and vertical tail between ONERA and AFDD/GIT results. The lower pressure coefficients for ONERA's results are in better agreement with experiment on the tail boom but not on the vertical tail. For the bottom centerline, the strut was not taken into account in the computations. The effect of applying tape to cover the gap between the strut and the fuselage can be observed by comparing the two experiments. The pressure coefficients are sensitive to the flow leakage. With the gap sealed by tape, the separation aft of the strut disappears in the F1 data. Here, the three computations predict neither the large separation at the

strut trailing edge due to the “flow suction” through the gap in S2Ch test, nor the pressure increase due to the strut leading edge stagnation.

### Force Comparison

Table 1 summarizes for the three partners the force coefficients for the standard isolated fuselage test case. ONERA’s results are essentially the same for the three turbulence models investigated. The standard  $k-\omega$  model provides the lowest drag and lift (absolute value), whereas it provides the highest drag and lift for AFDD. A notable exception is the AFDD Spalart-Allmaras result that shows a drag value 19% lower than the 2-equations models. A possible explanation for this discrepancy is the non-standard implementation of the Spalart-Allmaras model in OVERFLOW, which varies from the standard, published version used in *elsA* and FUN3D [20]. The effect is that transition is delayed at moderately low Reynolds number even when the turbulence model is turned on everywhere (“fully turbulent”). Such is the case with this configuration. An increased amount of laminar flow may account for some of the lower drag. The comparison between ONERA  $k-\omega$ , AFDD  $k-\omega$  and GIT Spalart-Allmaras is very good, except for lift (24% discrepancy between ONERA/AFDD and GIT values). Compared to the F1 experimental data, the absolute numerical values of drag, side and lift force are underestimated. In the wind tunnel test, the rotor hub drag is included, and both the strut and the rotor hub interact with the fuselage. Leakage around the strut which cannot be sealed due to interference with the balance measurements, also changes the fuselage lower surface flow field. At this point, these influences may explain the discrepancy between the numerical and experimental data.

**Table 1. Force coefficients for different turbulence models**

	$C_{DS}$ (x 1.e-02)	$C_{SS}$ (x 1.e-02)	$C_{LS}$ (x 1.e-02)
<b>ONERA</b>			
S-A	1.09	-1.18	-1.23
$k-\omega$	1.02	-1.20	-1.17
k-l	1.12	-1.18	-1.20
<b>AFDD</b>			
S-A	0.86	-1.19	-1.19
$k-\omega$	1.06	-1.21	-1.26
SST	1.02	-1.17	-1.14
<b>GIT</b>			
S-A	1.03	-1.20	-1.45
<b>F1 Exp.</b>	$1.42 \pm 0.13$	$-1.63 \pm 0.1$	$-2.68 \pm 0.28$

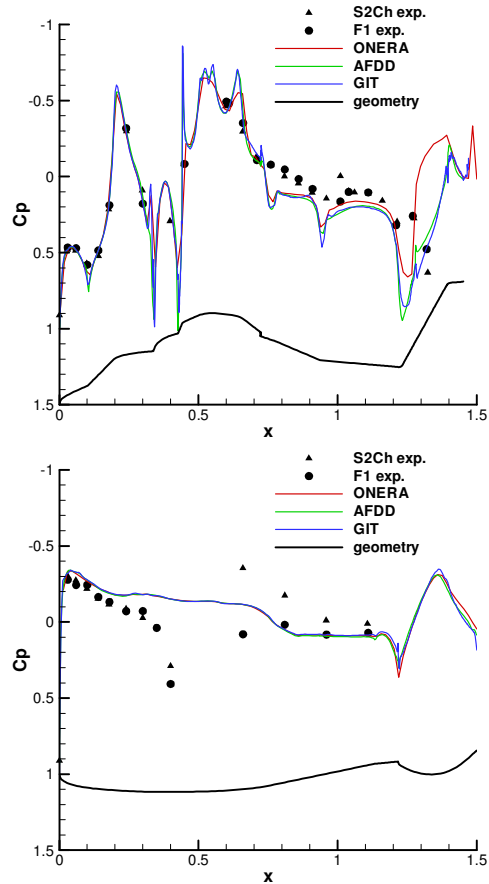


Figure 7. Comparison between partners of pressure coefficient for isolated fuselage

### Strut and Hub Effects

As discussed previously, the distribution of pressure coefficient is not well predicted in particular on the fuselage bottom due to the lack of the strut model. In addition, the rotor hub, which was present in the experiments, also may have an important influence on the drag force and the pressure coefficients. In this section, AFDD and GIT have examined the influence of the strut and hub geometries on the simulation. Although there were differences in the loads (cf. Table 1), the same turbulence model, Spalart-Allmaras, was chosen for consistency. The strut is a NACA0020 airfoil. The hub, while quite complex in reality, is modelled as a circular cylinder with convex top (cf. Fig. 8). Figure 9 shows pressure coefficients on the top and bottom centerlines. Both computations show an increase in  $C_p$  just aft of the rotor hub on the top centerline, denoting an improvement in the capture of the separated flows aft of the hub. On the lower centerline, the influence of the strut/fuselage stagnation point is captured via the rapid increase in  $C_p$  upstream of the strut. The smaller increase in  $C_p$  downstream of the strut is also predicted. The numerical results are now in much better agreement with F1 pressure data.

Table 2 presents the strut and hub effects on the force coefficients. Although the AFDD Spalart-Allmaras model was shown to underestimate the drag coefficient, AFDD and GIT computations with and without the strut and the hub components show consistent trends. Note that the force integration for the configuration with the hub and strut is performed over the fuselage and the hub, consistent with the F1 experiment. The drag is largely increased with the inclusion of the strut and the hub. AFDD shows a small lift increase, while GIT indicates a much larger lift loss. The side force increases also but by only 4%. The numerical results are then generally in better agreement with the F1 experimental data but there are still important discrepancies, in particular for the lift coefficient. As seen on the  $C_p$  distribution along the top centerline, the separation area aft of the engine fairing is not well captured and may explain the underestimation of the force coefficients.

**Table 2. Strut and hub influence on the force coefficients**

	$C_{DS}$ (x 1.e-02)	$C_{SS}$ (x 1.e-02)	$C_{LS}$ (x 1.e-02)
<b>AFDD</b>			
w/o strut+hub	0.86	-1.19	-1.19
with strut+hub	1.05	-1.27	-1.14
<b>GIT</b>			
w/o strut+hub	1.03	-1.20	-1.45
with strut+hub	1.33	-1.23	-1.68
<b>F1 Exp.</b>	1.42±0.13	-1.63±0.1	-2.68±0.28

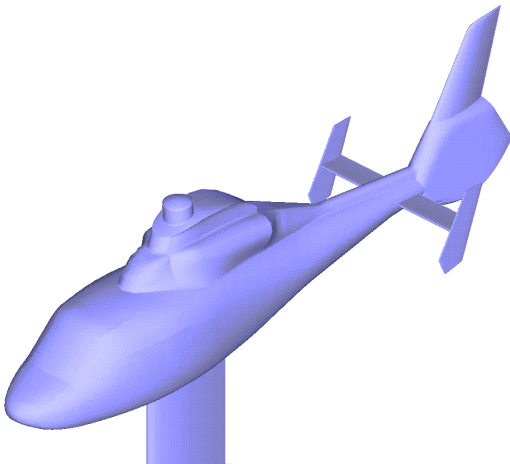


Figure 8. Dauphin fuselage with the wind tunnel support strut and a simplified rotor hub

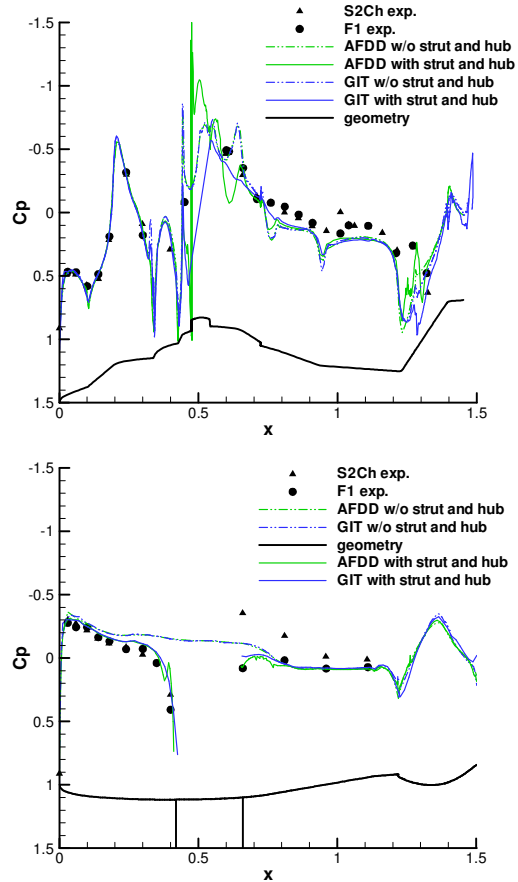


Figure 9. Effect of strut and hub on pressure coefficients along the top and bottom centerlines

### Sideslip Effects

A second test-case that has been chosen for the isolated fuselage analysis includes sideslip effects. The freestream velocity is now equal to 30 m/s and a sideslip angle of  $-5^\circ$  (nose right) is applied. The flow field around the Dauphin fuselage including the strut and rotor hub has been computed by AFDD and GIT with the Spalart-Allmaras turbulence model. Figure 10 presents the pressure distribution on the top and bottom centerlines. The behaviours of the two codes are similar and the numerical results are in good agreement with the F1 experimental pressure data. With respect to the standard flow conditions (with no sideslip angle), it should be noted that the predicted pressure values on the vertical tail are more negative when a sideslip angle is applied. The separation area aft of the engine fairing still is not well captured but the origin of this discrepancy is not yet understood.

Table 3 provides the force coefficients of AFDD and GIT computations along with the F1 experiment. With respect to the zero sideslip case (cf. Table 2), the experiment shows an increase in both drag (55%) and lift (17%). AFDD results show only small drag (6%) and lift (5%) increases, while GIT results show almost no drag change and a lift decrease (12%). Due to the sideslip angle (nose right), the sign of the side force changes. The side force is

in excellent agreement between CFD codes and the experiment. The noted lift and drag discrepancies between the numerical and experimental results require further investigations.

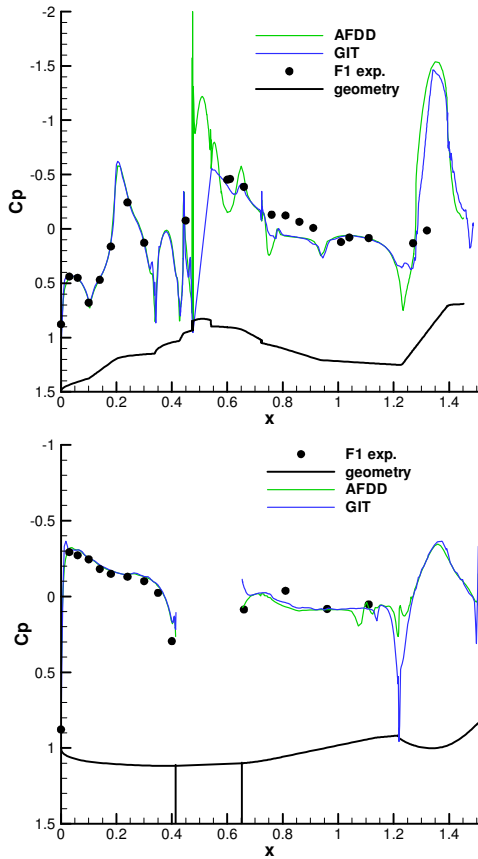


Figure 10. Sideslip effect on pressure coefficients along the top and bottom centerlines

**Table 3. Force coefficients for isolated fuselage with sideslip angle**

	$C_{DS}$ (x 1.e-02)	$C_{SS}$ (x 1.e-02)	$C_{LS}$ (x 1.e-02)
<b>AFDD</b>	1.11	3.59	-1.09
<b>GIT</b>	1.31	3.60	-1.89
<b>F1 Exp.</b>	2.20±0.04	3.57±0.09	-2.23±0.07

### Fuselage with Actuator Disk

Although there still remain questions about the pressure correlations aft of the rotor hub and lift and drag predictions, evaluations continued in order to determine the impact of the rotor on the fuselage. The test conditions used for the results with rotor are identical to the no sideslip case. The overall rotor thrust is  $200C_T/\sigma = 14.5$ . The actuator disk described earlier was utilized as the mechanism to introduce the rotor into the calculations.

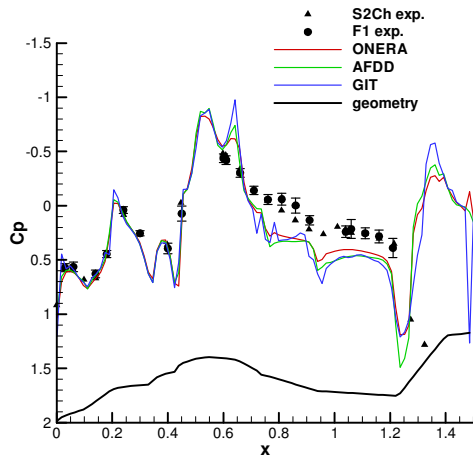
The impact of simulating both a uniform and a non-uniform actuator disk has been evaluated. Based on results from the isolated fuselage analyses, GIT CFD solutions with actuator disk use the Spalart-Allmaras turbulence model, AFDD solutions use a 2-equation model ( $k-\omega$  for uniform actuator disk, SST for non-uniform actuator disk), and ONERA uses the Smith  $k-l$  model.

### Uniform Actuator Disk

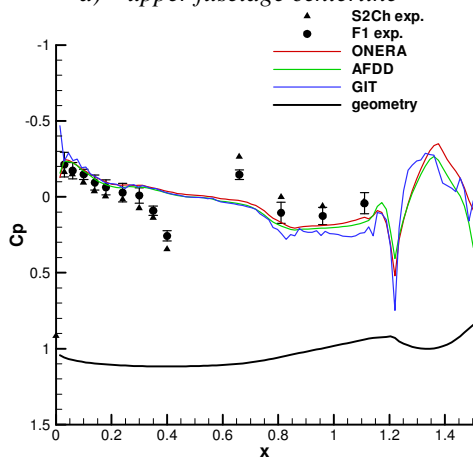
The uniform actuator disk was modelled using basic momentum theory to obtain the pressure jump for the mean rotor thrust. The constant pressure jump was applied to all of the grid points on the actuator disk surface for each of the three partner's grids. AFDD and ONERA both used low Mach preconditioning. GIT found that the compressible version of the FUN3D code was necessary to achieve stable solutions, though at the penalty of some surface variable smoothness and computational performance.

Figure 11 illustrates the pressure coefficients along the upper and lower fuselage centerlines with the addition of the uniform actuator disk. S2Ch and F1 experimental values are plotted: they are in good agreement, except in the separation area aft of the rotor hub, which is a sensitive zone of the model. Because the CFD configuration does not include the rotor hub or the strut, the numerical pressures show the same problems seen in Figure 7 for the isolated fuselage. As before, the change in the lower centerline pressure due to the stagnation point at the strut/fuselage intersection is not captured. Along the upper centerline, the characteristics behind the hub are also missed, although some recovery is seen by the simulations. On the upper fuselage centerline, ONERA appears to match the pressures on the tail boom slightly better than either AFDD or GIT. Notable are the differences in the upper centerline pressures due to the presence of the rotor, as visualized in Figures 7 and 11. The pressures on the nose are shifted by approximately  $0.5 \Delta C_p$ , indicating the influence of the rotor downwash in this area. All of the CFD codes predict this trend correctly. The downwash from the rotor also impacts the tail boom and vertical tail intersection, as seen by the increase in the stagnation pressure.

The surface pressure on the entire fuselage is shown in Figure 12. This figure confirms the centerline coefficient trends and also shows that the CFD simulations have all captured the same salient features of the surface pressures. The GIT pressure coefficients show some numerical oscillatory behaviour consistent with the compressible solution of the isolated fuselage. The GIT simulation shows the largest impact of the rotor downwash on the tail boom (high  $C_p$  values) and ONERA the smallest influence.



a) upper fuselage centerline



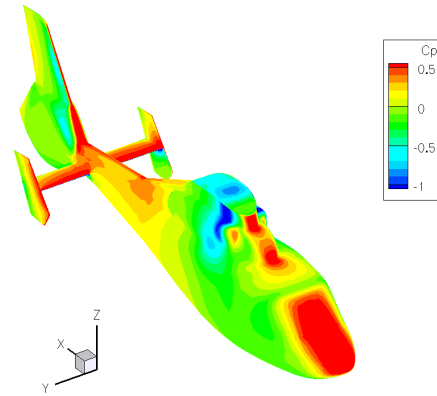
b) lower fuselage centerline

Figure 11. Comparison of fuselage centerline pressure coefficient with a uniform actuator disk

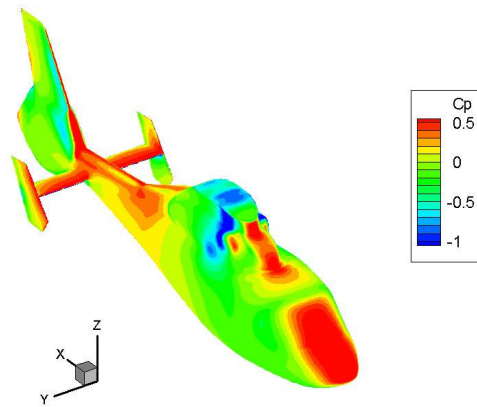
The forces predicted by the CFD simulations are provided in Table 4. As is readily apparent from Figures 11 and 12, the lift will be under predicted by the CFD simulations since the pressures indicate less suction over the tail boom and hub area. Differences in empennage calculations (vertical tail, vertical fins and horizontal tail) appear to be the primary cause for the differences between the CFD simulations, based on integrations without these components (not shown). This was verified as the cause of the differences in the isolated fuselage cases as well. In general ONERA and AFDD forces are in reasonable agreement with each other.

Table 4. Force coefficients for the uniform actuator disk

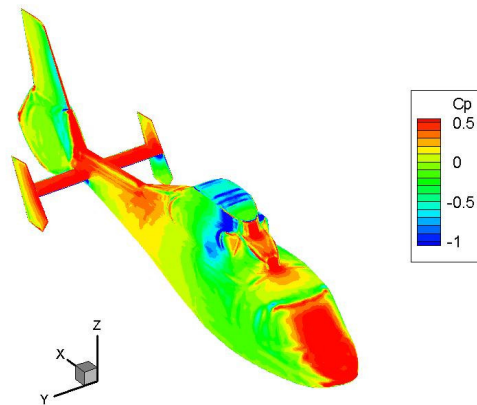
	$C_{DS}$ (x 1.e-02)	$C_{SS}$ (x 1.e-02)	$C_{LS}$ (x 1.e-02)
<b>ONERA</b>	1.30	-1.51	-3.86
<b>AFDD</b>	1.07	-1.62	-3.67
<b>GIT</b>	1.72	-2.02	-4.74
<b>S2Ch Exp.</b>	1.78	-0.55	-4.01



a) ONERA



b) AFDD



c) GIT

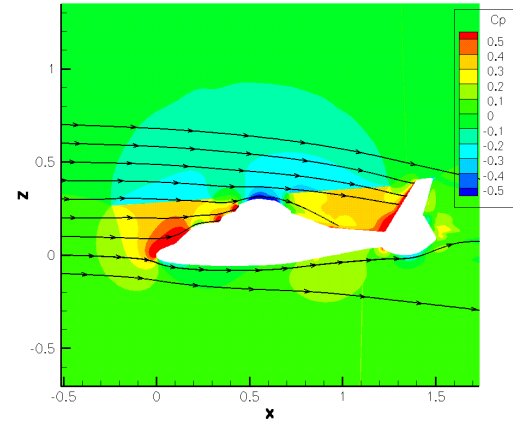
Figure 12. Comparison of fuselage surface pressure coefficient with a uniform actuator disk

ONERA and AFDD drag computations are lower than the experiment by 27% and 40% respectively, while the GIT drag is only 3% lower than the experimental drag. The three side force discrepancies are important compared with experiment, in particular for GIT. The cause of the

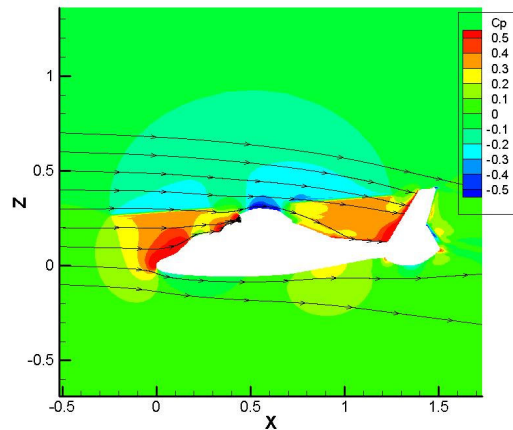
side force overprediction is apparent in Figure 12 and confirmed when the tail fins are removed from the calculation – they account for 50% of the side force. ONERA and AFDD lift computations are lower than the experiment by 4% and 8%, whereas the GIT lift is 18% higher than the experimental lift. An incompressible actuator disk formulation is needed in FUN3D (GIT) to alleviate these inconsistencies.

The pressures on the fuselage surface can be related to the downwash emanating from the rotor simulation. These are depicted in Figure 13 as streamlines superimposed on the flow field centerline pressure coefficient. The streamlines are computed by ignoring the out-of-plane velocity component. By comparing the streamlines from identical starting locations, the differences in the simulations can be assessed. The streamlines for all three simulations are quite similar for both the forward and aft regions. All of the simulations show streamlines that intersect with the vertical tail or tail boom at approximately the same locations. The streamline going just under the fuselage shows some differences near the tail: the ONERA streamline stays much closer to the surface wall, whereas the GIT and AFDD streamlines flow away from it. The ONERA pressure differences through the actuator disk condition are slightly lower than the other two simulations. The GIT and AFDD flow fields are very similar, with some differences in the flow field over the tail boom that are consistent with the surface centerline pressures from Figure 11.

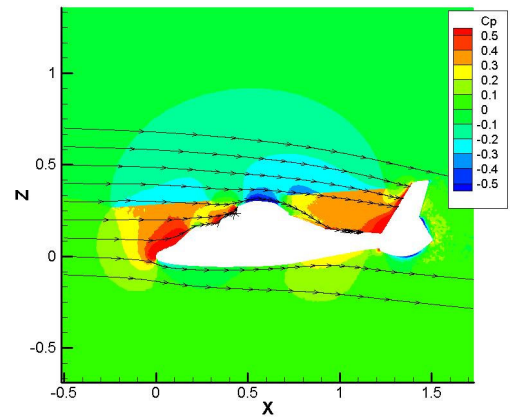
Streamwise vorticity contours are shown in Figure 14 for the CFD calculations at a streamwise station through the tail boom,  $x = 1.1375$ . Vorticity computed from Laser Doppler Velocimetry (LDV) measurements from the S2Ch experiment is also available for comparison. The general features of the vorticity are the same for all three simulations, although some small counter-rotating vortices can be seen for the AFDD data above the main rotor vortices. The main rotor vortices are largest for the GIT simulation, smallest for the AFDD simulation. The differences could be related to the grid density and numerical dissipation. The AFDD and ONERA contours are in particularly good qualitative agreement. Comparatively, the lower fuselage vortices in the GIT solution are of opposite sign. The vorticity for the uniform actuator disk is a mirror image about the  $y$  axis for the three simulations, as expected, and as such does not pick up the asymmetries in the experiment.



a) ONERA



b) AFDD



c) GIT

Figure 13. Streamlines superimposed on centerline pressure coefficient contours with a uniform actuator disk

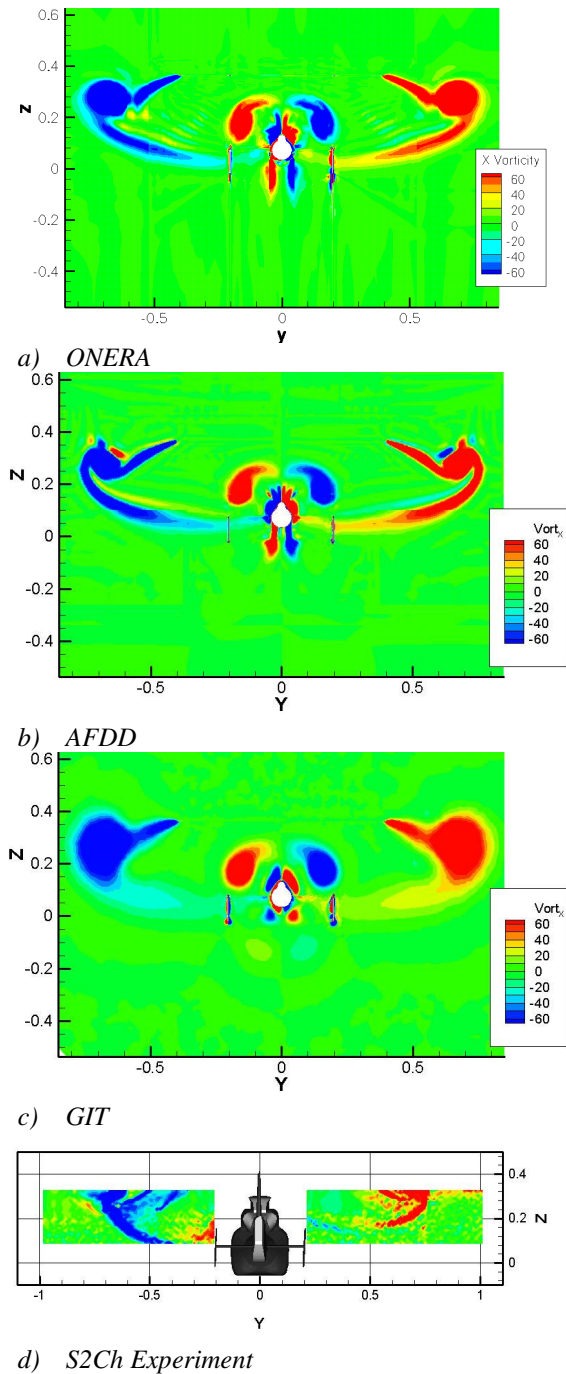


Figure 14. X-component of vorticity at  $x=1.1375\text{m}$  with a uniform actuator disk

#### Non-Uniform Actuator Disk

The non-uniform, varying actuator disk forces were obtained by running the HOST comprehensive code [21] with lifting line aerodynamics for the model test conditions. The normal component of the force generated by HOST is shown in Figure 15, but swirl is also included. By utilizing these inputs into the actuator disk, the asymmetric influence of the rotor on the fuselage can be captured.

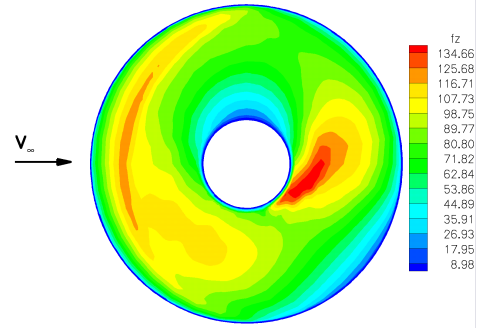


Figure 15. HOST prediction of the normal force for the Dauphin 365N rotor (Fig. 2, [22]).

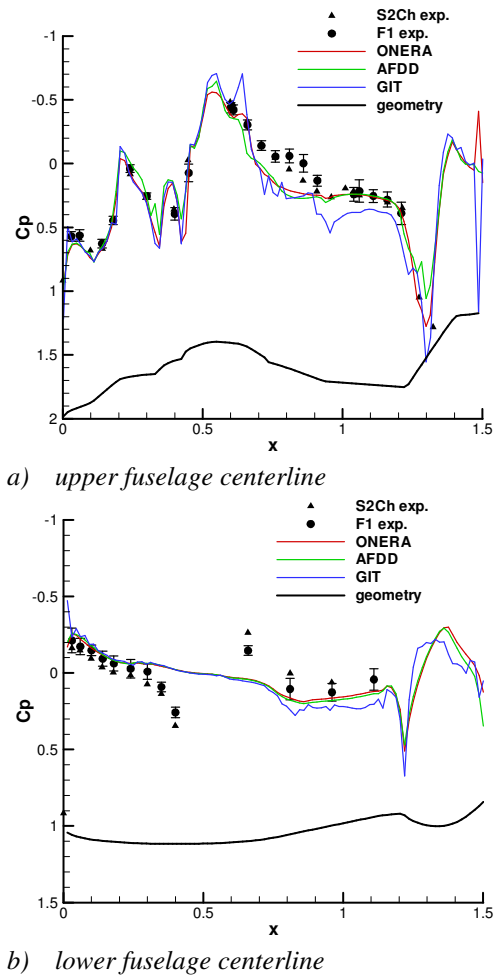


Figure 16. Comparison of fuselage centerline pressure coefficient with a non-uniform actuator disk

The pressure coefficients on the centerline of the fuselage are again compared in Figure 16. In conjunction with Figure 11, the influence of the non-uniform actuator disk can be compared with the uniform actuator disk. Overall, the same trends appear, but the aft separation/reattachment region is better predicted, in particular by AFDD and ONERA, which recover the

experimental pressures towards the aft end of the tail boom. The varying actuator disk also tends to drive the pressure coefficient predictions to more negative pressures at the vertical tail. ONERA and AFDD results are very similar, except on the front upper part of the fuselage ( $0.2 < X < 0.4$ ) where AFDD pressure is lower than the two others. GIT results are higher aft of the hub and on the tail boom. The differences between the lower centerline pressure predictions using the two rotor models are indistinguishable.

The differences in the impact of the uniform and non-uniform actuator disk are visible when Figures 12 and 17 are compared. The suction on the top of the fuselage is greatly diminished. The pressure decreases over the upper portion of the tail boom, but GIT values remains higher than the others, as seen in Figure 16. The asymmetry of the flow over the fuselage is particularly obvious on the ONERA forward fuselage. Note that the rotor is turning clockwise. Overall, the three simulations are again qualitatively similar in that the salient features of the flow are captured.

The data in Table 5 indicate some notable changes in the forces on the fuselage. The ONERA, AFDD and GIT drags have now increased by 8%, 41% and 8% respectively. GIT drag has moved from 3% lower than the experimental value to 4% higher. Again ONERA and AFDD predictions are in generally good agreement with each other. The AFDD drag is now within 15% of the experimental value. The culprit for these large drag increases appears to be the tail pressure predictions, which are now higher. The lift values increase for all the simulations and underestimate the experimental value, in particular by 26% for ONERA. The side forces have decreased slightly, but remain significantly different than experiment.

**Table 5. Force coefficients for the varying actuator disk**

	$C_{DS}$ (x 1.e-02)	$C_{SS}$ (x 1.e-02)	$C_{LS}$ (x 1.e-02)
<b>ONERA</b>	1.41	-1.79	-2.95
<b>AFDD</b>	1.51	-1.72	-3.18
<b>GIT</b>	1.86	-2.26	-3.65
<b>S2Ch Exp.</b>	1.78	-0.55	-4.01

The rotor downwash can again be related to the surface pressure to explain the differences in the features (Figure 18). Except for some oscillations of the isocontours of  $C_p$  in the AFDD flow at the front lower part of the actuator disk, ONERA and AFDD results are similar. The flow over the forward fuselage in the ONERA and AFDD simulations is strong enough that additional flow goes to the aft fuselage and provides the energy to reattach the separated flow. The high pressure region is confined to just forward of the vertical tail. The GIT aft flow field below the rotor shows larger regions of high pressure,

correlating with the separated region over the tail boom. The streamlines for the three simulations intersect with the vertical tail at the same locations. The GIT simulation provides higher pressure under the actuator disk than either the ONERA or AFDD simulations.

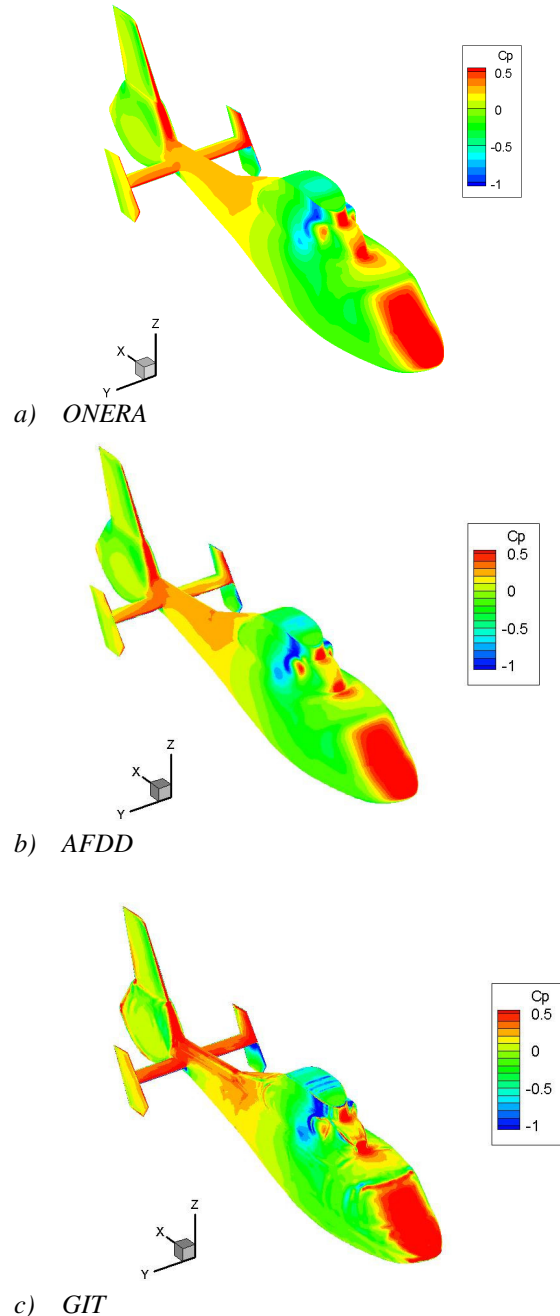
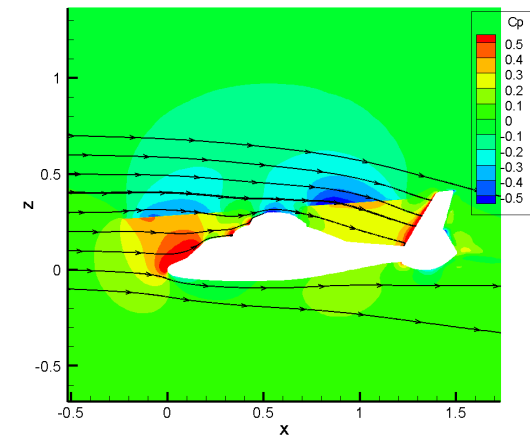
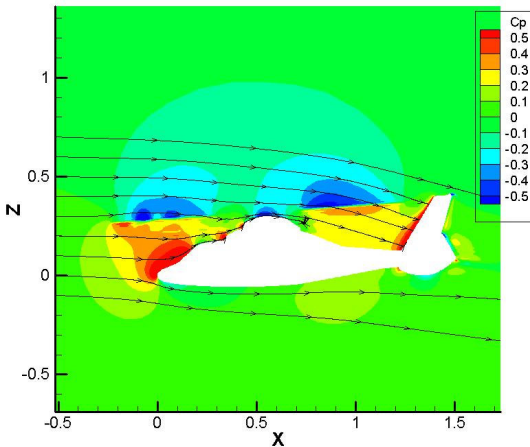


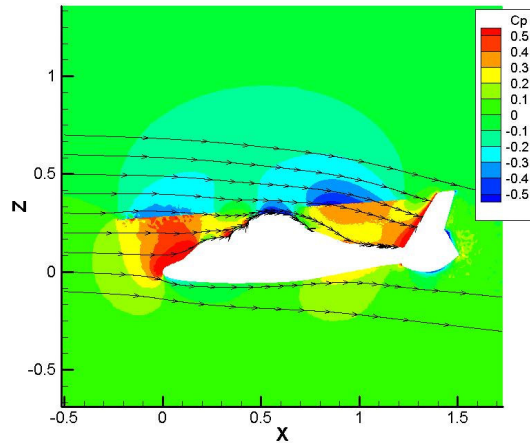
**Figure 17. Comparison of fuselage surface pressure coefficient with a non-uniform actuator disk.**



a) ONERA



b) AFDD

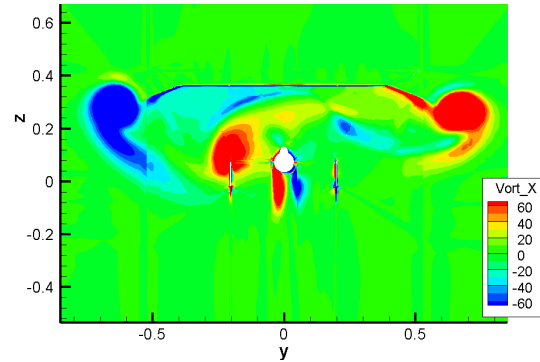


c) GIT

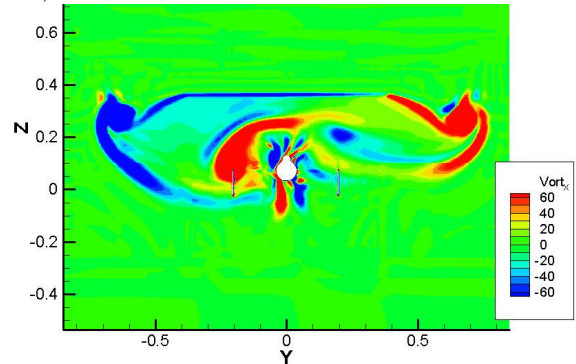
Figure 18. Streamlines superimposed on centerline pressure coefficient contours with a non-uniform actuator disk

With the addition of the non-uniform rotor model, the vorticity has become very complex and asymmetric compared with the uniform rotor model. Vorticity through the rotor disk is seen. On Figure 19, the left root vortex has moved downward and interacts with the left vertical fin. The three flow fields show the same relative motion of the vortices, although the GIT vortices tend to be larger

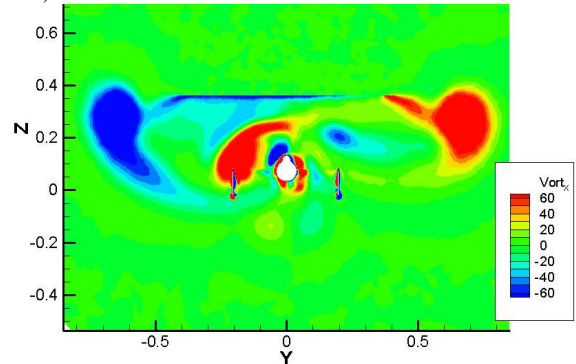
as noted previously. The lower right fuselage vortex in the GIT simulation has completely disappeared as the lower left vortex moves towards the right. The other two simulations still have a distinct vortex in that region. Both AFDD and GIT show vortices just over the tail boom, whereas they have disappeared in ONERA simulation.



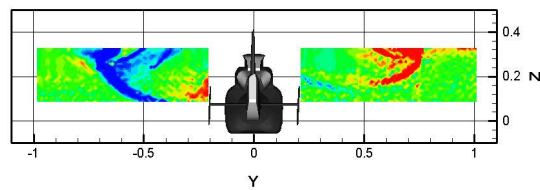
a) ONERA



b) AFDD



c) GIT



d) S2Ch experiment

Figure 19. X-component of vorticity at  $x=1.1375m$  with a non-uniform actuator disk

The flow features correlate qualitatively with the S2Ch experimental data. The vorticity from the left tip is seen to descend faster than the right. Negative vorticity beneath the left side of the rotor disk is captured in all solutions and seen in the LDV data. Also, the distortion of the root vortices is similar, to the extent that they appear in the data. However, in comparison with the experiment, the wakes and vortices in the CFD appear to be descending faster.

## CONCLUSIONS

Three different flow solvers (*elsA*, OVERFLOW, and FUN3D) using three meshing strategies (structured multiblock, structured overset, and unstructured) have been compared on a Dauphin 365N helicopter configuration in low speed forward flight. An isolated fuselage has been investigated for grid density, turbulence model, compressibility, and sideslip effects. Steady rotor-fuselage calculations have been performed with uniform and non-uniform actuator disks. Comparisons were made with pressure coefficient data, fuselage forces, and LDV flow visualization from the ONERA S2Ch and F1 wind tunnels. The following conclusions are made:

- Isolated fuselage pressures and forces are insensitive to the choice of one- or two-equation turbulence models.
- Grid convergence of the isolated fuselage forces was obtained with particular attention to surface resolution. This does not necessarily imply that grid convergence was obtained for simulations using an actuator disk due to significant rotor-fuselage interactions near the empennage. A refinement may be required in particular for the vertical tail and fin regions (as they appear to be the source of discrepancies in loading) and in the actuator disk vortical flow regions.
- For the low speed flight condition studied here,  $V_\infty=15$  m/s, low Mach number preconditioning or an incompressible formulation is required for an accurate (force prediction) and smooth solution.
- The sideslip effect is correctly captured only for the side force coefficient.
- With or without a rotor, good fuselage pressure coefficient agreement with data is obtained, except in the region behind the rotor hub. Good correlation on the fuselage lower surface requires modelling of the wind tunnel support strut. The strut and the hub influences are confirmed by improvement of the force comparisons with experiment. Careful attention must be paid to experimental strut-fuselage interactions.
- A uniform actuator disk model fails to accurately model the rotor-fuselage flow field.
- A non-uniform actuator disk model correctly captures fuselage pressures and qualitatively models the time-averaged rotor and fuselage vorticity flow field.

- Fuselage force prediction is generally in agreement between CFD codes, although certain discrepancies exist. Good correlation with data has not been obtained partially due to inaccurate modelling of the experimental configuration. Further investigation of CFD and experimental data is required in this area.

The objective of such a comparative study is the simulation of a complete helicopter and the next step towards this goal will be unsteady computations of the helicopter fuselage and the rotor blades. The new experimental PIV F1 data will then be compared to the numerical simulations.

## ACKNOWLEDGEMENTS

The authors would like to acknowledge Arnaud Le Pape (ONERA) for providing the experimental data. The authors are grateful to Eurocopter for the Dauphin 365N geometry. The GIT authors would like to acknowledge the support provided by the National Rotorcraft Technology Center (NTRC) at the Georgia Institute of Technology. Dr. Yung Yu is the technical monitor of this center. Computational support for the NTRC was provided through the DoD High Performance Computing Centers at ERDC and NAVO through an HPC grant from the US Army, S/AAA Dr. Roger Strawn. For the AFDD and GIT calculations, the computer resources of the Department of Defense Major Shared Resource Centers (MSRC) are gratefully acknowledged.

## REFERENCES

1. P. Buning, D. Jespersen, D. C., T. Pulliam, W. Chan, J. Slotnick, S. Krist, and K. Renze  
*OVERFLOW User's Manual, Version 1.8*  
NASA Langley Research Center, 1998.
2. W. Chan, R. Meakin, and M. Potsdam  
*CHSSI Software for Geometrically Complex Unsteady Aerodynamic Applications*  
AIAA Paper 2001-0593, AIAA 39<sup>th</sup> Aerospace Sciences Meeting and Exhibit, Reno, NV, January 2001.
3. P. Buning  
*Consolidation of Time-Accurate, Moving Body Capabilities in OVERFLOW*  
<http://www.arl.hpc.mil/Overset2002>  
6<sup>th</sup> Overset Composite Grid and Solution Technology Symposium, Fort Walton Beach, FL, October 2002.
4. D. Jespersen, T. Pulliam, P. Buning  
*Recent Enhancements to OVERFLOW*  
AIAA Paper 1997-644, AIAA 35<sup>th</sup> Aerospace Sciences Meeting and Exhibit, Reno, NV, January 1997.

5. Y.H. Choi, C. L. Merkle  
*The application of preconditioning to viscous flows*  
Journal of Computational Physics, 105, pp. 207-233, 1993.
6. *Manuel théorique elsA version 1.6*  
ONERA, 2002.
7. C. Benoît, M.-C. Le Pape, G. Jeanfaivre  
*Improvement of the robustness of the Chimera method*  
32<sup>nd</sup> AIAA Fluid Dynamics Conference & Exhibit, Saint-Louis, USA, June 2002.
8. F. Le Chuiton  
*Actuator disk modelling for helicopter rotors*  
28<sup>th</sup> European Rotorcraft Forum, Bristol, UK, September 2002.
9. N. Bettschart  
*Rotor-fuselage interaction: Euler and Navier-Stokes computations with an actuator disk*  
55<sup>th</sup> Annual Forum of the American Helicopter Society, Montreal, Canada, May 1999.
10. J. Brezillon  
*Simulation of rotor-fuselage interactions by using an actuator disk*  
26<sup>th</sup> European Rotorcraft Forum, The Hague, Netherlands, September 2000.
11. W. Anderson and D. Bonhaus,  
*An Implicit Upwind Algorithm for Computing Turbulent Flows on Unstructured Grids*  
Computers & Fluids Vol. 23, No. 1, p. 1-21, 1994.
12. W. Anderson, R. Rausch, and D. Bonhaus  
*Implicit/Multigrid Algorithms for Incompressible Turbulent Flows on Unstructured Grids*  
J. of Comp. Physics No. 128, p 391-408, 1996.
13. D. Bonhaus  
*An Upwind Multigrid Method for Solving Viscous Flows on Unstructured Triangular Meshes*  
M.S. Thesis, George Washington University, 1993.
14. A. Chorin  
*A Numerical Method for Solving Incompressible Viscous Flow Problems*  
J. of Comp. Physics No. 2, p12-26, 1967.
15. P. Roe  
*Approximate Riemann Solvers, Parameter Vectors and Difference Schemes*  
J. of Comp. Physics No. 43, p 357-372, 1981.
16. I. Fejtek and L. Roberts  
*Navier-Stokes Computation of Wing/Rotor Interaction for a Tilt Rotor in Hover*  
AIAA Journal. Vol. 30 No. 11, p 2595-2603, 1992.
17. S. Pirzadeh  
*Three-Dimensional Unstructured Viscous Grids by the Advancing Layers Method*  
AIAA Journal, Vol. 34, No. 1, Jan. 1996, pp. 43-39.
18. *Gridgen User Manual, Version 13.3* Pointwise, Inc, Bedford, TX, 2003.
19. A. Le Pape, J. Gatard, J.-C. Monnier  
*Experimental investigations of rotor-fuselage aerodynamic interactions using a helicopter powered model*  
to be published at the 30<sup>th</sup> European Rotorcraft Forum, Marseilles, France, September 2004.
20. E. Lee-Rausch, P. Buning, D. Mavriplis, J. Morrison, M. Park, S. Rivers, and C. Rumsey  
*CFD Sensitivity Analysis of a Drag Prediction Workshop Wing/Body Transport Configuration*  
AIAA Paper 2003-3400, 21st AIAA Applied Aerodynamics Conference, Orlando, FL, June 2003.
21. B. Benoît, A.-M. Dequin, K. Kampa, W. Grunhagen, P.-M. Basset, B. Gimonet  
*HOST, a general helicopter simulation, tool for Germany and France*  
56<sup>th</sup> Annual Forum of the American Helicopter Society, Virginia Beach (USA), May 2002.
22. T. Renaud, C. Benoît, J. -C. Boniface, P. Gardarein  
*Navier-Stokes computations of a complete helicopter configuration accounting for main and tail rotors effects*  
29<sup>th</sup> European Rotorcraft Forum, Friedrichshafen, Germany, September 2003.